Appl. Phys. B 42, 193–213 (1987)

Applied Physics B Photophysics and Laser Chemistry

© Springer-Verlag 1987

Correlation Techniques in Dynamic Light Scattering

K. Schätzel

Institut für Angewandte Physik, Universität, D-2300 Kiel, Fed. Rep. Germany

Received 13 October 1986/Accepted 21 December 1986

Abstract. The motion of small scatterers in a laser beam results in Doppler shifts of the scattered light. Various homodyne or heterodyne experiments may be used to measure such shifts. The stochastic nature of spatial particle arrangements and of the photon-detection process leads to statistic data processing schemes like temporal correlation or the computation of structure functions. Photon correlation is one of these schemes and has found numerous applications in velocimetry and Brownian motion studies. Topics of current interest are dead-time corrections, the use of photon structure functions, and multiple tau measurements, which access large ranges of time constants in a single run.

More recent data processing techniques are recurrence rate correlation for the immediate determination of velocity correlation functions in seeded fluid flows and the measurement of amplitude-weighted phase structure functions, which is able to resolve very small particle displacements otherwise completely obscured by random Brownian motion. Rate correlation found applications in hydrodynamic studies of the route to turbulence, while the major use of phase structure function processing is a very significant increase in the sensitivity of electrophoretic mobility measurements by light scattering.

PACS: 05.40.+6, 47.80.+v, 06.50.Dc

Moving scatterers like seed particles in a flow, macromolecules undergoing Brownian motion, or local fluctuations of the refractive index in a fluid, generally produce a Doppler shift, i.e. they scatter light at a frequency slightly different from the illuminating wave. Since such scatterers typically move at velocities slower than the speed of sound, which lies some 6 decades below the speed of light, the relative frequency change is rather small, e.g. $10^{-6} \ldots 10^{-15}$.

If optical path differences in the scattering experiment do not exceed a few mm or some 10^4 wavelengths (for visible light), such small frequency shifts produce no considerable change of wavelength. Light propagation may be calculated correctly, if we assume identical wavelengths for incident and scattered light – the assumption of quasi elastic light scattering (QELS).

As a second consequence of the relative smallness of terrestrial Doppler shifts, most times they cannot be resolved by classical spectrometers like gratings or etalons. The typical shift frequencies between 1 Hz and some 100 Mhz are, however, well within reach of direct electronic processing, and the technique of light-beating spectroscopy or intensity interferometry may be applied [1–4].

Even though this technique was introduced by Hanbury-Brown and Twiss as early as 1956 [5], it was not until the invention of the laser as a strong coherent source of illumination that QELS and intensity interferometry were used to study the motion of small particles. Sensitivity and efficiency of experiments were considerably increased when Pike's group at Malvern developed photon correlation [6, 7]. This technique provides quantum limited single photon counting sensitivity together with real-time performance and digital precision of the electronic signal processor.

Photon-correlation spectroscopy found two major fields of applications: laser velocimetry, particularly in large wind tunnels, and particle sizing by measurement of diffusive Brownian motion [1–4]. The latter technique experiences a continuing growth of applications in many branches of biology, chemistry, and physics ranging from industrial production control to fundamental studies on interacting particle systems.

High-power lasers or large-aperture scattering geometries often provide signal intensities well above the dead time limit [8] of photon-counting detectors. The common use of neutral-density filters cures the problem, but at the expense of increased shot noise.

Furthermore, the availability of analog signals with good signal-to-noise ratio allows novel signal processing techniques to be applied, which may be used to extract information about dynamic properties of the scattering system beyond those obtainable by photon correlation.

An example is recurrence rate correlation, based on threshold crossing events of an optical intensity, which provides temporal velocity correlation information about the motion of scattering particles. Rate correlation was invented by Erdmann at Seattle [9, 10] and further developed and applied to periodic and chaotic flows by our group at Kiel [11–16].

Completely new light scattering experiments are feasible, if the signal processing is based on the phase rather than the intensity of Doppler shifted light. My first application was the study of turbulent random phase screens as a model of atmospheric wave propagation [17–20].

More recently, I developed a signal processing scheme involving amplitude weighted phase structure functions (AWPS). The AWPS technique allows the measurement of extremely small collective particle motion otherwise completely obscured by diffusive random motion. Our major application is the light scattering study of electrophoretic mobilities with significantly increased sensitivity [21–23].

Even though all these dynamic light scattering techniques, particularly photon correlation, have been described in many separate publications, this paper appears to be the first one presenting the various techniques in their common optical and statistical context. Quite clearly, space does not permit a complete review of all the relevant work in the field. In fact, for the most recent technique, AWPS, some relevant work has not been completed yet.

Still I hope that a coherent and up-to-date summary of three dynamic light scattering techniques – photon correlation, rate correlation, and AWPS – may provide a useful orientation to readers new to the field as well as broaden the view of those already familiar with some light scattering experiments.

Because all techniques discussed in this paper make use of similar optical scattering setups and statistical data processing schemes, I will start with two fundamental sections which cover these topics in a general manner. Three more specific sections will then apply our general concepts to specific experiments and discuss particular problems and applications.

1. Optical Setups

Dynamic light scattering experiments are performed with many different optical setups. They may be roughly classified into experiments with a single illuminating laser beam and experiments with two interfering beams in the measurement volume. Further differences arise due to the use of coherent and incoherent detection schemes. Finally we may discuss single or multi particle scattering.

1.1. Single Beam Setup

a) Single Particle Scattering. Illumination of a point-like particle by a focused laser beam is commonly (and quite well) approximated as plane-wave illumination characterized by an initial wave vector $\mathbf{k}_i$. A small detector in the far field selects a single direction of the scattered light field to be described by a final wave vector $\mathbf{k}_f$. The assumption of quasi-elastic light scattering corresponds to neglection of the very small length difference between $\mathbf{k}_i$ and $\mathbf{k}_f$. For a laser wavelength λ in the medium we assume

$$|\mathbf{k}_i| = |\mathbf{k}_f| = 2\pi/\lambda . \tag{1}$$

Particle motion over a distance small compared to the diameter of the illuminating beam causes negligable amplitude changes at the detector, but significant phase changes will be produced, if the motion $\mathbf{x}(t)$ has a nonzero component perpendicular to the bisector of $\mathbf{k}_i$ and $\mathbf{k}_f$. We obtain a complex amplitude at the detector

$$u_D(t) = a(\mathbf{x}(t)) \exp[\mathrm{i}(\mathbf{k}_i - \mathbf{k}_f)\mathbf{x}(t)] \tag{2}$$

which depends on the scattering geometry through the difference of the initial and final wave vectors only. This difference is the scattering vector commonly denoted by

$$\mathbf{q} = \mathbf{k}_i - \mathbf{k}_f . \tag{3}$$

Its magnitude depends on the wavelength and the scattering angle ϑ between $\mathbf{k}_i$ and $\mathbf{k}_f$,

$$|\mathbf{q}| = (4\pi/\lambda)\sin(\vartheta/2), \tag{4}$$

and may vary between 0 and $4\pi/\lambda$, corresponding to virtual fringe separations down to one half of the illuminating wavelength. In practice, it is often difficult to obtain good signals at very small scattering angles and values below 5° are rarely used in dynamic light scattering.

Since photodetectors are sensitive to optical intensities only, the phase change in (2) cannot be observed by the simple setup of Fig. 1. In order to produce significant intensity changes, a single scattering particle must move a distance comparable to the illuminating beam radius, which happens on much longer time scales than those required for significant phase changes. The shape of the intensity signal is governed by the beam profile, typically close to a Gaussian for gas lasers. The measurement of number fluctuations in

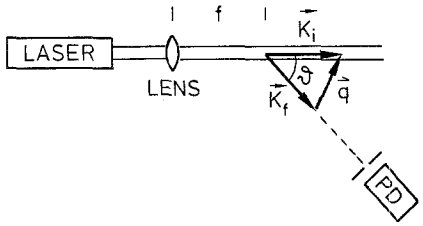

Fig. 1. Schematic setup for single-beam scattering consisting of laser, focusing lens, detection aperture, and detector, typically a photomultiplier tube

photon correlation as well as single-beam rate correlation are based on such comparatively slow intensity changes.

Particle diameters which are not small compared to the wavelength complicate the computation of the absolute magnitude of the amplitude factor a in (2), but do not change the general form of this equation. The dependence of a on the scattering angle ϑ is the central topic of static light scattering and exceeds the scope of this paper. The same restriction holds for polarization effects like depolarized scattering. We will assume light that is linearly polarized perpendicularly to the scattering plane, simplifying our calculations to scalar complex scattering amplitudes.

b) Many Particle Scattering. Working with coherent illumination, the complex amplitudes scattered by all the particles in the measurement volume add up at the detector and we obtain the resultant amplitude

$$u_D = \sum_{j=1}^{N} a(\mathbf{x}_j(t)) \exp[i\mathbf{q}\mathbf{x}_j(t)], \tag{5}$$

where j labels the individual scattering particles. Eq. (5) may be interpreted as a random-walk problem in the complex plane and for independent stochastic particle positions (noninteracting particles) the central limit theorem predicts Gaussian statistics for the detector amplitude in the large N or many particle limit (Fig. 2).

Again, we are unable to measure a small collective particle motion with the single beam setup of Fig. 1. Identical phase changes of each particle's complex amplitude result in a pure phase change of u_D – a simple rotation of the random walk graph (Fig. 2) in the complex plane.

However, particle motions relative to each other will produce phase as well as amplitude or intensity changes in u_D. The single-beam setup is hence suitable to determine velocity gradients [30, 31] or – a particularly important application – Brownian motion. In this context, the single-beam setup is commonly referred to as homodyne scattering experiment.

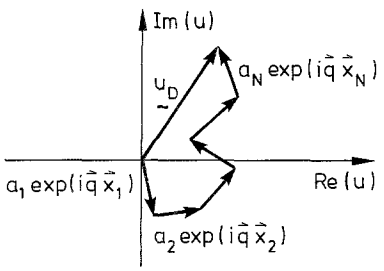

Fig. 2. Coherent multi particle scattering as a random walk in the complex plane

1.2. Dual-Beam Setups

a) Reference-Beam Technique. In order to detect phase fluctuations in the scattered light, we need an interferometer. The simplest possible change of the single beam arrangement in Fig. 1 is the addition of two beam splitting mirrors to create a reference beam with wave vector identical to $\mathbf{k}_f$ (Fig. 3).

The same result may be achieved by a single beam splitter plus a mirror (Fig. 4), a more commonly used setup which provides easier alignment.

If u_R denotes the fixed complex amplitude of the reference beam at the detector, we obtain a detector intensity

$$I_D(t) = |u_D(t)|^2 = |u_R|^2 + 2\,\mathrm{Re}\left\{u_R^* \sum_{j=1}^{N} a_j(\mathbf{x}_j(t)) \exp[i\mathbf{q}\mathbf{x}_j(t)]\right\} + \left|\sum_{j=1}^{N} a_j(\mathbf{x}_j(t)) \exp[i\mathbf{q}\mathbf{x}_j(t)]\right|^2. \tag{6}$$

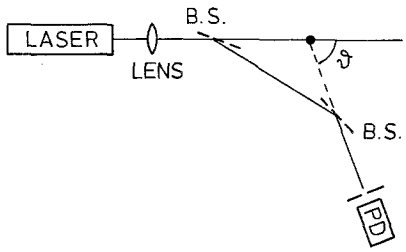

Fig. 3. Schematic reference beam setup with two beam splitters (B.S.)

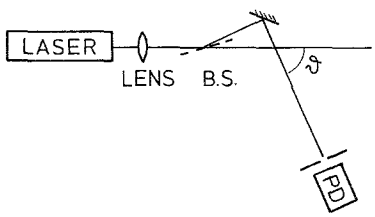

Fig. 4. Schematic reference beam setup with a single beam splitter (B.S.)

The last term in (6) is typically neglected for reference amplitudes large compared to the scattered amplitude, and the cross term dominates the dynamic (i.e., time dependent) part of the detected signal.

The reference beam or heterodyne setups provide high sensitivity to collective as well as relative particle motions. Applications are velocimetry, mobility studies, and again Brownian motion.

b) Real-Fringe Technique. Instead of mixing or heterodyning a scattered beam with a constant reference beam on the detector, interference may be produced just as well by mixing of light that is scattered from two illuminating beams (Fig. 5) which cross under an angle ϑ. Application of (2) yields a detected intensity

$$I_D(t) = |u_D(t)|^2 = 2|a(x(t))|^2 \{1 + \cos[\mathbf{q}_1 \mathbf{x}(t) - \mathbf{q}_2 \mathbf{x}(t)]\} \quad (7)$$

for single particle scattering where

$$\mathbf{q}_1 = \mathbf{k}_{i1} - \mathbf{k}_f$$

and

$$\mathbf{q}_2 = \mathbf{k}_{i2} - \mathbf{k}_f$$

denote the two scattering vectors. Because (7) depends on the difference,

$$\mathbf{q} = \mathbf{q}_1 - \mathbf{q}_2 = \mathbf{k}_{i1} - \mathbf{k}_f - \mathbf{k}_{i2} + \mathbf{k}_f = \mathbf{k}_{i1} - \mathbf{k}_{i2}, \quad (8)$$

of these scattering vectors only, the scattered intensity remains independent of the detection direction or $\mathbf{k}_f$.

This independence is easily understood if we look upon the two illuminating beams in Fig. 5 as producing real interference fringes in the measurement volume. These fringes are parallel to the bisector of the two beams and have a spacing of

$$s = 2\pi/|\mathbf{q}| = \lambda/2 \sin(\vartheta/2). \quad (9)$$

Motion of a scattering particle perpendicular to these fringes results in a sinusoidal modulation of the scattered light with the Doppler frequency

$$\nu_D = \dot{x}(t)/s = q\dot{x}(t)/2\pi, \quad (10)$$

given by the ratio of the relevant velocity component and the fringe spacing.

Particle motion all the way across the measurement volume causes a low-frequency change in $|a|^2$, in addition to this sinusoidal modulation. For constant particle velocity we obtain the characteristic Doppler bursts of laser Doppler velocimetry. Figure 6 shows such a burst for the simplest case of particle motion perpendicular to the fringes and right through the center of the measurement volume.

c) Coherent and Incoherent Detection. So far we have neglected finite aperture effects of the detector, i.e. we assumed a single final wave vector $\mathbf{k}_f$. Quite clearly, a vanishing detector aperture implies vanishing signal intensity and is of no use for any practical purpose. In order to reduce shot noise, we would like to use as large a detector aperture as possible.

Many setups used for quasi-elastic light scattering, however, do not tolerate large apertures. Many particle homodyne as well as reference beam experiments require coherent addition of complex amplitudes scattered by all particles inside the measurement volume. Hence their mutual optical phase differences should not vary by more than a small fraction of 2π across the detector aperture. For a measurement volume of diameter d, this coherence condition limits detection apertures to a cone characterized by the coherence angle

$$\lambda/d. \quad (11)$$

With $\lambda = 0.5$ μm and $d = 0.5$ mm we obtain an angle of 0.001 rad corresponding to a detector aperture smaller than 0.2 mm, if the detector is placed 200 mm away from the measurement volume. The very small amount of scattered light which passes such a small detector aperture is responsible for the widespread use of single photon counting detection in QELS.

If detector apertures are increased beyond one coherence cone, averaging of the speckle pattern in the detector plane reduces the contrast or the useful modulation of the detected signal. At large apertures, this reduction is proportional to the square root of the aperture area. This is exactly the same rate by which relative shot noise decreases with increasing aperture. Hence, larger apertures do not produce any gain in signal-to-noise ratio. In practice, detector apertures are kept within the order of one coherence area to avoid unnecessary dead time saturation of photon count rates.

Still, there exist other dynamic light scattering experiments, which do allow incoherent, large apar-

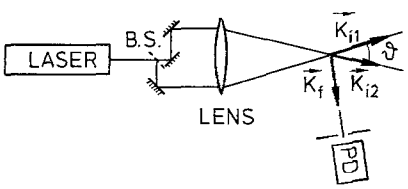

Fig. 5. Schematic symmetric real-fringe setup

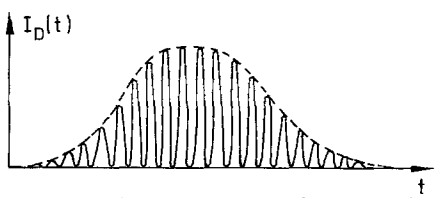

Fig. 6. Typical laser Doppler burst signal

ture detection without loss of contrast. Our discussion of single particle scattering in the symmetric dual beam or real fringe geometry showed, that the detected intensity did not depend on the scattering angle or $\mathbf{k}_f$ (at least for point-like scatterers). Hence, an increase of the detector aperture simply increases the useful signal instead of producing a large constant background due to speckle averaging – the problem of coherent detection schemes.

Loosely speaking, the coherence requirement of QELS has been shifted from the receiver to the transmitter side of the real-fringe experiment. The strong analog signals, which can often be achieved by large aperture incoherent detection, made the real-fringe technique the most popular one for laser Doppler velocimetry. It allows the use of inexpensive analog processors to measure Doppler frequencies in real time.

Furthermore, the high signal quality offered by incoherent detection experiments allows the application of new signal processing schemes like rate correlation and the measurement of phase structure functions, which are covered in the last sections of this paper.

An occasional problem of incoherent detection should not be overlooked, however. While the addition of complex amplitudes scattered by an arbitrarily large number of particles in the measurement volume did not reduce the signal contrast in coherent detection experiments, the addition of intensities in incoherent detection tends to build up a useless and often disturbing constant background. This background grows proportional to the number of scatterers N while the useful fluctuations grow like the square root of N only, due to random phase addition. The low-frequency background is typically removed by analog high pass filtering. There is, however, no possibility to remove its shot noise contribution in the signal frequency band. This noise again grows like the square root of N and we realize that incoherent detection experiments do not profit from an increased number of scattering particles in the measurement volume.

Since incoherent detection often allows the use of detector apertures of the order of 10000 coherence areas, only extreme particle concentrations – in this case more than 10000 per measurement volume – result in a signal-to-noise advantage of reference beam setups. Such concentrations are rare in velocimetry applications but may well occur in diffusion studies on concentrated suspensions.

2. Statistics for Dynamic Light Scattering

The stochastic nature of many particle light scattering as well as of light detection suggests the use of statistical concepts to extract physical information from dynamic light scattering experiments. This section summarizes useful concepts like correlation and structure functions of doubly stochastic random processes, some important model distributions, and more specific problems like noise considerations and dead time distortions.

2.1. Correlation of Doubly Stochastic Processes

Signals considered in dynamic light scattering are typically doubly stochastic processes, where properties of a fluctuating physical quantity like light intensity (photon correlation) or particle velocity (rate correlation) are to be determined from measurements of a second quantity like the rate of photon detections (photon correlation) or of threshold crossing events (rate correlation). The first or underlying quantity $x(t)$ typically constitutes a continuous stochastic process which governs certain statistical properties of the second discrete process $n(t)$, a number of pulses counted during a sampling interval of length t_s centered at a time t. Quite naturally, we will restrict our attention to discrete times t, which are integer multiples of t_s (Fig. 7).

The relations between the two processes $x(t)$ and $n(t)$ simplify considerably if we assume that $x(t)$ changes slowly as compared to the sample time clock interval t_s. In this limit, the continuous process $x(t)$ is well approximated by the discrete values it takes on at the clock times. Since t_s is typically chosen small enough in practical correlation experiments, we will accept this approximation throughout this paper.

Correlation measurements of doubly stochastic processes use two fundamental properties satisfied by many such processes. Firstly, we assume a linear relationship between the the expectation of $n(t)$ and the instantaneous value of the underlying process $x(t)$. If $\langle A|B\rangle$ denotes the conditional expectation of A given B, this linearity condition reads

$$\langle n(t)|x(t)\rangle_n = Cx(t). \tag{12}$$

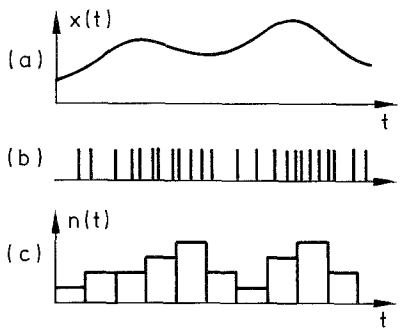

Fig. 7a–c. Example of (a) a continuous process $x(t)$, (b) derived sequence of events, and (c) the resulting discrete process $n(t)$

The index n is used to stress the fact that averaging is restricted to fluctuations of $n(t)$ for a fixed value of $x(t)$. C is a constant which can often be made equal to 1 by a proper choice of units.

As a second condition we require statistical independence of counts $n(t)$ and $n(t+\tau)$ for arbitrary but fixed values $x(t)$ and $x(t+\tau)$ of the underlying process. From this independence condition we obtain a conditional expectation

$$\langle n(t)n(t+\tau)|x(t),x(t+\tau)\rangle_n = \langle n(t)|x(t)\rangle_n \langle n(t+\tau)|x(t+\tau)\rangle_n . \quad (13)$$

Our two fundamental conditions immediately yield the important relation between the temporal correlation functions of the two processes,

$$\begin{aligned} G_n(\tau) &= \langle n(t)n(t+\tau)\rangle \\ &= \langle\langle n(t)n(t+\tau)|x(t),x(t+\tau)\rangle_n\rangle_x \\ &= \langle\langle n(t)|x(t)\rangle_n \langle n(t+\tau)|x(t+\tau)\rangle_n\rangle_x \\ &= C^2\langle x(t)x(t+\tau)\rangle_x = C^2 G_x(\tau) . \end{aligned} \quad (14)$$

$\langle\ldots\rangle_x$ denotes averaging over the underlying process. The use of the letter G for correlation functions is defined in (14). If necessary to avoid confusion, the process which is correlated is denoted by an index.

It should be stressed that beyond our two fundamental conditions of linearity (12) and independence (13), we did not need any further assumptions to derive the central relation (14). Particularly, we did not have to specify certain distributions for $x(t)$ or $n(t)$. This generality will, however, be lost if we compute more complicated properties of doubly stochastic processes and we will introduce important distribution models like Poisson, Gaussian, and Gamma processes in later sections.

Since the autocorrelation of $x(t)$ may be Fourier transformed to obtain the power spectral density – the well known Wiener-Khintchine theorem – spectral information about $x(t)$ may be determined from the measured correlation of $n(t)$. This idea of "time domain spectroscopy" is the basis of many applications of correlation techniques in dynamic light scattering.

2.2. Structure Function

While correlation functions are the most widely used concept to describe the temporal behavior of stochastic processes, comparable information is contained in the mean square change of the process, now known as its structure function [24],

$$D_x(\tau) = \langle [x(t)-x(t+\tau)]^2\rangle . \quad (15)$$

In spite of the similarity of wording, this structure function has no relation to the so called structure factor which describes anglular scattering cross sections in static light scattering.

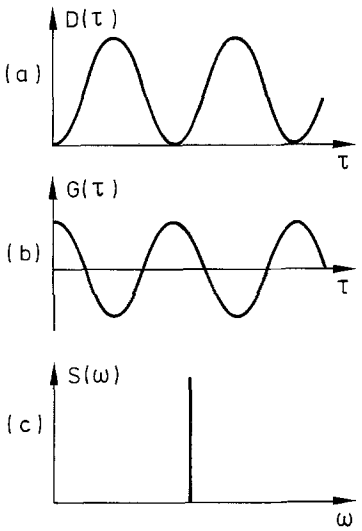

Fig. 8. (a) structure function, (b) correlation, and (c) power spectrum of a sinusoidal periodic signal

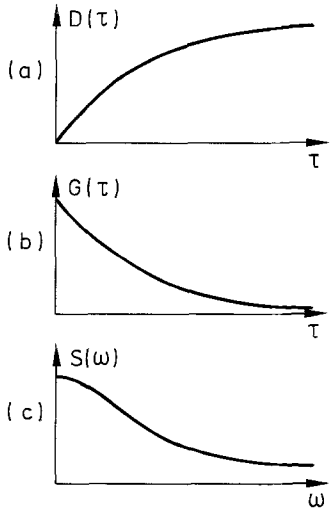

Fig. 9. (a) structure function, (b) correlation, and (c) power spectrum of a Lorentzian random process

For stationary processes $x(t)$, correlation and structure functions are connected by

$$D_x(\tau) = 2\langle x(t)^2\rangle - 2\langle x(t)x(t+\tau)\rangle = 2G_x(0) - 2G_x(\tau) . \quad (16)$$

Essentially, structure functions are correlograms turned upside down. Eq. (16) and the Wiener-Khintchine theorem [66] may be used to transform a structure function into a power spectrum. Figures 8 and 9 show two examples.

While structure functions are just a possible alternative to correlations for stationary processes, they are the only possible choice to characterize non-stationary processes with stationary increments, for which corre-

lation functions cannot be defined. Examples for such processes are Brownian motion and many optical phase signals.

For later reference we state Einstein's famous result for the mean square displacement of a particle due to diffusion in one dimension [67],

$$D_x(\tau)=\langle[x(t)-x(t+\tau)]^2\rangle=2D\tau\,. \tag{17}$$

D denotes the constant of diffusion and we recognize (17) as the structure function of the particle position $x(t)$.

Finally, we calculate the structure function of our doubly stochastic process $n(t)$. Under the validity of the two fundamental conditions of linearity (12) and independence (13), we obtain

$$\begin{aligned}D_n(\tau)&=\langle n(t)^2-2n(t)n(t+\tau)+n(t+\tau)^2\rangle\\&=\langle[n(t)^2-\langle n(t)|x(t)\rangle_n^2]+[n(t+\tau)^2\\&\quad-\langle n(t+\tau)|x(t+\tau)\rangle_n^2]+[\langle n(t)|x(t)\rangle_n^2\\&\quad-2\langle n(t)|x(t)\rangle_n\langle n(t+\tau)|x(t+\tau)\rangle_n\\&\quad+\langle n(t+\tau)|x(t+\tau)\rangle_n^2]\rangle_x=\langle\mathrm{Var}[n(t)|x(t)]\rangle_x\\&\quad+\langle\mathrm{Var}[n(t+\tau)|x(t+\tau)]\rangle_x+C^2D_x(\tau)\,.\end{aligned} \tag{18}$$

In comparison with (14) we find an additional background term equal to the sum of the conditional variances of $n(t)$ averaged over $x(t)$ at the two times t and $t+\tau$. Caution, these conditional variances are not equal to the variances of $n(t)$, but always smaller than these. For stationary $x(t)$, the two conditional variances are equal and the background does not depend on the lag time.

This background shifts the structure function of $n(t)$ to higher values and must often be subtracted out prior to further processing. Two schemes may be used. First, we may extrapolate $D_n(\tau)$ towards the lag time zero to obtain the background. This scheme makes use of the continuity of the structure function of a continuously differentiable random process.

The second scheme requires explicit knowledge of the statistics of $n(t)$ to compute the conditional variance in (18). This calculation is still independent of the statistics of $x(t)$. In order to proceed with this scheme we must now focus our interest on model distributions.

2.3. Stochastic Models

While the Poisson process, which is characteristic for independent point events, clearly constitutes the most important candidate for our discrete process $n(t)$, a large number of models may be treated for the statistics of the underlying continuous process $x(t)$. Saleh [32] gave a detailed discussion of several such models. Our attention will be restricted to a single model, the Gamma distribution, only, which includes the popular Gaussian process as well as the exponential distribution as limiting cases.

a) Poisson Process. The number of photons detected within a sampling interval of constant light intensity as well as the number of non-interacting point particles in a measurement volume are Poisson distributed random variables. Hence, the Poisson process will suffice as a model for $n(t)$ in most dynamic light scattering applications.

Let us, for simplicity, assume that the constant of proportionality in (12) equals 1 and omit unnecessary time arguments. The assumption of Poisson statistics for $n(t)$ then reads

$$P(n|x)=x^n\exp(-x)/n! \tag{19}$$

with conditional factorial moments

$$\langle n(n-1)\ldots(n-m+1)|x\rangle=x^m\,. \tag{20}$$

For $m=1$, (20) immediately yields our linearity condition (12).

Averaging over the – still unspecified – statistics of $x(t)$ yields the Poisson transform of the density $p_x(x)$,

$$P(n)=\int_0^\infty x^n\exp(-x)p_x(x)dx/n! \tag{21}$$

with factorial moments

$$\langle n(n-1)\ldots(n-m+1)\rangle=\langle x^m\rangle\,, \tag{22}$$

equal to the ordinary moments of x. Equation (22) is frequently used to obtain moments of x from measured histograms of n.

If the counts $n(t)$ are statistically independent for non-overlapping sampling intervals, we may compute higher-order correlations of $n(t)$. Up to fourth order, these mixed moments are required to calculate the estimator variances of measured correlograms and structure functions. Writing n_1 for $n(t_1)$, x_1 for $x(t_1)$, δ_{12} for $\delta(t_1,t_2)$, etc., and omitting the time index where it is not really required, we obtain [32, 26]

$$\langle n\rangle=\langle x\rangle\,, \tag{23}$$

$$\langle n_1n_2\rangle=\langle x_1x_1\rangle+\delta_{12}\langle x\rangle\,, \tag{24}$$

$$\begin{aligned}\langle n_1n_2n_3\rangle&=\langle x_1x_2x_3\rangle+\delta_{12}\langle x_1x_3\rangle+\delta_{23}\langle x_1x_2\rangle\\&\quad+\delta_{13}\langle x_1x_2\rangle+\delta_{123}\langle x\rangle\,,\end{aligned} \tag{25}$$

$$\begin{aligned}\langle n_1n_2n_3n_4\rangle&=\langle x_1x_2x_3x_4\rangle+\delta_{12}\langle x_1x_3x_4\rangle\\&\quad+\delta_{13}\langle x_1x_2x_4\rangle+\ldots+\delta_{123}\langle x_1x_4\rangle\\&\quad+\delta_{124}\langle x_1x_3\rangle\\&\quad+\ldots+\delta_{1234}[3\langle x^2\rangle+\langle x\rangle]\,.\end{aligned} \tag{26}$$

The Poisson character of the counting statistics shows up, whenever two or more of the considered (discrete) times coincide. For the ordinary second-order auto-

correlation (24), this leads to an additional contribution at zero lag time, which becomes large as compared to the rest of the correlogram at small mean count rates.

In photon correlation applications, this zero spike may be avoided by cross correlation of the signals from two detectors, which are optically superposed by means of a beam splitter. This scheme reduces afterpulsing problems, as well [33].

With Poisson statistics for $n(t)$, the conditional variance in (18) yields

$$\mathrm{Var}(n|x)=\langle n(n-1)|x\rangle+\langle n|x\rangle-\langle n|x\rangle^2=x=\langle n|x\rangle, \tag{27}$$

amounting to a background equal to twice the mean count rate, which may easily be corrected in digital structure functions.

b) Gamma Process. Intensity statistics in dynamic light scattering generally depend on the geometry of the measurement volume [34, 35]. This dependence, however, vanishes in the limit of many independent particles (or particle clusters), where the central limit theorem predicts Gaussian statistics for the complex amplitude scattered into a coherent detector aperture.

Gaussian amplitudes yield exponential intensity statistics [32]. Real experiments generally show narrower intensity distributions, because of the finite real detector area discussed in Sect. 1.2c. The effect of partial coherence may be modelled by adding independent exponentially distributed intensities originating from the individual speckle areas within the detector aperture, which leads to a Gamma distributed sum intensity [32]. The probability density and the generating function of a Gamma distribution are

$$p(x)=(x/\beta\langle x\rangle)^{1-1/\beta}\exp(-x/\beta\langle x\rangle)/\beta\langle x\rangle\Gamma(1/\beta), \tag{28}$$

$$\langle\exp(-sx)\rangle=(1+\beta\langle x\rangle s)^{-1/\beta}. \tag{29}$$

The moments are

$$\langle x^m\rangle=\langle x\rangle^m(1)(1+\beta)(1+2\beta)\ldots[1+(m-1)\beta], \tag{30}$$

particularly,

$$\langle x^2\rangle=\langle x\rangle^2(1+\beta). \tag{31}$$

The distribution parameter β may be recognized from (31) as the relative contrast or the degree of coherence of the signal or the "intercept" of the correlogram. $1/\beta$ denotes a number of degrees of freedom, – in dynamic light scattering easily identified with the number of independent speckles in the detector aperture.

In order to compute correlation and structure functions, we need the joint distribution at two times or its generating function,

$$\langle\exp[-sx(t)-s'x(t+\tau)]\rangle = [(1+\beta\langle x\rangle s)(1+\beta\langle x\rangle s')-\beta^2\varrho^2\langle x\rangle^2 ss']^{-1/\beta}, \tag{32}$$

which contains the temporal correlation coefficient $\varrho(\tau)$ as a parameter. (32) yields a correlation function

$$\langle x(t)x(t+\tau)\rangle=\langle x\rangle^2[1+\beta\varrho(\tau)^2]. \tag{33}$$

Since $\varrho(\tau)$ does not need to be specified, arbitrary shapes of the correlogram may be generated by the Gamma model.

The final discussion of two special cases will further illustrate the generality of our model. For $\beta=1$, the density (28) is just an exponential density. This case of perfect coherence is obtained for the intensity statistics of the widely used quasi-thermal or Gaussian light.

For very small values of β, infinite divisibility of the Gamma distribution and the central limit theorem predict an approach towards a Gaussian distribution with mean $\langle x\rangle$ and variance $\beta\langle x\rangle^2$. In this limit, the Gamma model may even serve to describe many particle reference beam experiments.

2.4. Noise Considerations

The usefulness of structure functions and correlation functions is largely determined by their noise performance. For a doubly-stochastic process, two separate sources of noise must be considered.

Firstly, random fluctuations of $n(t)$ about its expectation $Cx(t)$ cause a counting noise. This type of noise is known as photon noise in photon counting experiments and may be associated with fluctuations of the particle arrival rate in rate-correlation experiments. It dominates at small count rates (less than 1 per sample time) and is easily recognized in measurements, because it shows up as random scatter of the measured values in the various lag time channels of a structure function or correlogram.

Much less obvious – but equally important – than wide bandwidth counting noise, are the typically band limited fluctuations of the underlying signal $x(t)$, which result in "signal noise" that is highly correlated in adjacent channels. Its dominance at high count rates yields smooth measured curves, which, however, appear to be badly reproducible in repeated measurements.

The fundamental calculation of both types of noise for photon correlation functions of a Gauss-Lorentz light, i.e. of light with Gaussian amplitude statistics and Lorentzian spectrum, was carried out by Jakeman et al. [37, 38]. They found a slight decrease of the single channel estimator variance with increasing lag time, and a pronounced increase of this variance with decreasing mean count rates – the photon noise regime. Above some 10 counts per coherence time, noise levels saturate – photon noise becomes negligable, as compared to signal noise.

Both types of noise are also treated in [26] where I compared the noise of normalized photon correlation as well as photon structure functions for the same case of Gauss-Lorentz light. Both, homodyne and heterodyne experiments with perfectly coherent detection were treated.

Correlation functions generally show less sensitivity to wide bandwidth counting noise. Exponentially distributed $x(t)$ yields a ratio up to $\sqrt{5}$ on favor of the standard deviation of correlograms. For Gaussian $x(t)$, this ratio is reduced to $\sqrt{3}$ [25, 26].

Signal noise, however, with its typical narrow bandwidth, affects structure functions less than correlograms. In contrast to correlograms, structure functions show a pronounced decrease of their estimator variance at small lag times for high count rates [26]. As a consequence, reliable information about fast signal components may be obtained by structure functions within shorter measurement times than by correlograms.

Furthermore, computer simulations [25] as well as theoretical considerations [26] indicate better stability of structure functions to very short total measurement times. Similar advantages exist for drifting signals and signals with a large constant background [24].

2.5. *Dead Time Distortions*

A typical systematic error of all counting systems is due to dead time effects which are caused by finite response times of the detector or the counting electronics. Dead time effects are particularly annoying, because their presence violates both of our fundamental conditions.

While deviations from linearity due to dead time saturation are limited to high count rates, which must be a significant fraction of the inverse dead time, the independence condition does not hold even at small count rates, if we consider lag times comparable to the dead time.

a) Paralyzability. For quantitative dead time investigations, we must specify the type of dead time behavior in our system. Well suited for theoretical studies are two limiting cases.

In one limit, any input event blocks the system for a certain dead time, no matter whether the particular event fell within some other input event's dead time period or not. Such a system becomes completely blocked at very high count rates and is therefore called paralyzable. Examples are single beam rate correlation experiments or photon counting photomultipliers with ideal Schmitt-trigger type discriminators.

Monostable pulse shaping circuitry and the input counters of digital correlators, however, are better modelled by the other limiting case of nonparalyzable systems. This type of systems simply ignores input events, which fall into a dead period, without further extension of this period. The output event rate approaches the inverse dead time for very large input event rates. Figure 10 illustrates both cases.

b) Dead-Time Effects in Correlograms. In contrast to the large number of papers dealing with dead-time distortions of single-time photon counting statistics (references in [8, 32]), calculations of correlation distortions seem to have been restricted to first order approximations [32, 40] or exotic cases of clipped correlograms [41], until my recent studies of dead time effects in photon correlation [8] and structure [42] functions of doubly stochastic Poisson type input processes.

These studies showed that the problem is most easily solved for the case of a paralyzable system. For such a system, the probability of an output event depends on the number of input events falling into one dead time interval immediately preceding the output event considered, but not on any events further back in time. If this number is zero, the output event has the same probability as the corresponding input event. If this number exceeds zero, the probability of the output event vanishes. Integration over the sampling intervals of width t_s, separated by a lag time τ yields the conditional expectation of the digital correlation for given values of the underlying process $x(t)$ or – for the sake of brevity – x_t,

$$\langle n_0 n_\tau | x_0 x_\tau \rangle = C^2 x_0 x_\tau \exp[-C(x_0 + x_\tau) t_d/t_s] f(\tau, t_d, t_s) \quad (34)$$

with

$$f(\tau, t_d, t_s) = \begin{cases} 1 & \text{for } \tau > t_d + t_s, \\ 1 - (t_d + t_s - \tau)^2/2t_s^2 & \text{for } t_d + t_s > \tau > t_d, \\ (\tau + t_s - t_d)^2/2t_s^2 & \text{for } t_d > \tau > t_d - t_s, \\ 0 & \text{for } t_d - t_s > \tau. \end{cases} \quad (35)$$

Equation (34) replaces (13) and shows both, saturation nonlinearity in the exponential function, and statistical dependence in the factor f, because of paralyzable system dead time t_d.

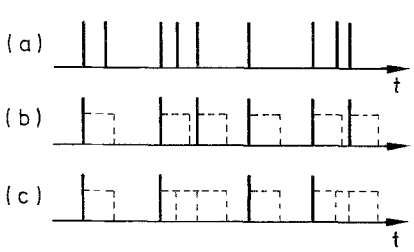

Fig. 10. (a) signal without dead time and signals of a (b) nonparalyzable or a (c) paralyzable system

For nonparalyzable systems, the region where f deviates from unity extends beyond the sum of dead time and sample time. Furthermore, this factor now depends on the count rate [8]. The exponential nonlinearity in (34) gets replaced by terms like [8, 32]

$$(1+Cx_t t_d/t_s)^{-1}. \tag{36}$$

Obviously, dead time effects depend on the statistics of the underlying process $x(t)$. Using the fairly general Gamma model of Sect. 2.3b, the paralyzable system yields a normalized dead time distorted correlation

$$g_n(\tau)=\langle n_0 n_\tau\rangle/\langle n\rangle^2 = f(\tau, t_d, t_s)$$

$$\times \frac{1+\beta(1-2\varepsilon-2\beta\varepsilon^2)(1+\beta\varepsilon)^{-2}\varrho^2+\beta^2\varepsilon^2(1+\beta\varepsilon)^{-2}\varrho^4}{[1-\beta^2\varepsilon^2(1+\beta\varepsilon)^{-2}\varrho^2]^{2+1/\beta}} \tag{37}$$

ε is used as a dimensionless measure of the input count rate times the dead time,

$$\varepsilon = C\langle x\rangle t_d/t_s. \tag{38}$$

The nonparalyzable case is not easily computed in closed form, but may be well approximated by a paralyzable system with a dead time distributed at values

$$(2\pm\sqrt{2})t_d \tag{39}$$

with weights

$$(2\mp\sqrt{2})/4, \tag{40}$$

which is a tractable problem [8]. This approximation holds over much larger ranges of ε than power series expansions because the latter possess asymptotic convergence only.

c) Dead-Time Effects in Structure Functions. In addition to the same distortions as in correlograms, digital structure functions of Poisson processes show another dead time effect due to the presence of single time second moments in (18). Since dead times tend to narrow counting distributions, the second-order moment in the relation between structure function and correlation,

$$\langle(n_0-n_\tau)^2\rangle = 2\langle n^2\rangle - 2\langle n_0 n_\tau\rangle, \tag{41}$$

falls below the value obtained for a true Poisson process. The usual normalization by subtraction of

$$\langle n^2\rangle = C^2\langle x^2\rangle + C\langle x\rangle \tag{42}$$

must be replaced by subtraction of the corresponding dead time corrected moment [42].

In the paralyzable case, this moment reads [39, 8]

$$\langle n^2\rangle = C(1-2t_d/t_s+t_d^2/t_s^2)\langle x^2\exp(-2Cx)\rangle + C\langle x\exp(-Cx)\rangle \tag{43}$$

for dead times t_d below the sampling time t_s. For larger dead times, the first term on the right-hand side of (43) vanishes.

With the Gamma model of Sect. 2.3b, (43) may be computed as [42]

$$\langle n^2\rangle = C^2(1-2t_d/t_s+t_d^2/t_s^2)\langle x\rangle^2(1+\beta)(1-2\beta\varepsilon) + C\langle x\rangle(1+\beta\varepsilon) \tag{44}$$

for dead times smaller than the sample time.

Corresponding considerations for nonparalyzable systems lead to

$$\langle n^2\rangle = C^2\langle x^2/(1+Cxt_d/t_s)^2\rangle + C\langle x/(1+Cxt_d/t_s)^3\rangle \tag{45}$$

and, with a Gamma process for x and power series expansion in ε [42],

$$\langle n^2\rangle = C\langle x\rangle^2(1+\beta)[1-2(1+2\beta)\varepsilon + 3(1+2\beta)(1+3\beta)\varepsilon^2] + C\langle x\rangle[1-3(1+\beta)\varepsilon + 6(1+\beta)(1+2\beta)\varepsilon^2] + O(\varepsilon^3). \tag{46}$$

Without knowledge of the counting statistics, structure functions of stationary processes may be converted to correlations, if a monitor channel actually measures $\langle n^2\rangle$. This scheme works even in the presence of dead times. My digital structurator/correlator [28, 43, 44] computes $\langle n^2\rangle$ in place of the zero lag time channel of the structure function, which is zero by definition and hence redundant.

3. Photon Correlation

Following our summaries of the basic optical designs and statistical concepts useful in dynamic light scattering, we start the description of specific applications with photon correlation – certainly the best known and most widely used one of the signal processing schemes in quasi-elastic light scattering.

Many optical setups, as discussed in Sect. 1, require the use of coherent detection. This implies small detection angles and hence low light levels at the detector. Single-photon counting with its essentially quantum-limited noise performance has long become the standard technique for the measurement of weak scattered light signals.

The digital nature of single-photon counting pulses makes them well suited for processing by digital correlators, which offer a large dynamic range and absence of distortion or processing noise. In fact, it was only after the invention of Malvern's classic single bit correlator [6, 7], that intensity spectroscopy had its real breakthrough.

We will proceed with sketches of the two major applications of photon correlation today, the study of Brownian motion for particle sizing and the measure-

ment of flow velocities by light scattering from tracer particles.

3.1. Brownian-Motion Studies

Brownian motion of suspended particles, e.g. macromolecular solutions, or even thermal diffusion of fluctuations of the local refractive index in pure liquids, result in a system of many scatterers, which move relative to each other. In Sect. 1.1 we showed that such a relative motion produces intensity fluctuations of the light scattered from a single probing laser beam into a coherent (small) detector aperture. The fact that the single beam or homodyne setup is insensitive to collective motion of the scatterers yields high stability against convection or vibration problems and has made the homodyne technique very popular in many branches of physics, chemistry, and biology.

a) Amplitude Correlation. The principle of diffusion measurements by light scattering is most easily explained by considering amplitude or so called first order correlation functions. From (5) we may compute them as

$$\begin{aligned} G_1(\tau) &= \langle u_D(0) u_D^*(\tau)\rangle \\ &= \left\langle \sum_{j=1}^{N}\sum_{m=1}^{N} a_j a_m \exp[\mathrm{i}\mathbf{q}\mathbf{x}_j(0) - \mathrm{i}\mathbf{q}\mathbf{x}_m(\tau)]\right\rangle \\ &= N\langle |a|^2\rangle \langle \exp[\mathrm{i}\mathbf{q}\Delta\mathbf{x}_j(\tau)]\rangle , \end{aligned} \tag{47}$$

if we assume statistical independence of the scatterers, i.e. neglect particle interactions, and assume identical particles or monodisperse suspensions. Furthermore, we make use of the usual assumption of slowly varying absolute single particle amplitudes, which allows us to perform phase averages separately. Equation (47) depends on the lag time τ through the average particle displacement $\Delta x(\tau)$ only, which Einstein found to be normally distributed with variance (17) or

$$\langle \Delta x(\tau)^2\rangle = 2D\tau , \tag{48}$$

true for lag times large compared to hydrodynamic relaxation times. Computation of the average in (47) thus amounts to taking the Fourier transform into q-space of the Gaussian particle displacement density and yields

$$G_1(\tau) = N\langle |a|^2\rangle \exp(-q^2 D\tau), \tag{49}$$

an exponential decay with a time constant from which we may obtain D, the constant of diffusion. This exponential correlation corresponds to a Lorentzian spectrum. Typical time constants or bandwidths are between 1 Hz and 1 MHz, indeed very small as compared to optical frequencies. This is the reason for the great success of time domain spectroscopy in diffusion measurements.

Using the Stokes-Einstein relation [67],

$$D = kT/(6\pi\eta a), \tag{50}$$

where k denotes Boltzmann's constant, T the absolute temperature, and η the viscosity of the solvent, we may calculate the particle radius a from measured diffusion constants D. Thus we have an optical technique to determine sub-wavelength particle sizes. Possible applications are studies of solid particles, macromolecules, emulsion droplets, micelles, and a large number of microbiological systems in the size range between several *nm* and some 1 μm or more.

b) Intensity Correlation. While amplitude or first-order correlations are most easily computed, all photon correlation experiments really yield intensity or second-order correlation functions only. With the assumptions used in Sect. 3.1a, we quickly obtain the intensity or photon correlation

$$\begin{aligned} G_2(\tau) &= \langle n(0)n(\tau)\rangle = \langle u_D(0)u_D^*(0)u_D(\tau)u_D^*(\tau)\rangle \\ &= \left\langle \sum_{j=1}^{N}\sum_{m=1}^{N}\sum_{p=1}^{N}\sum_{q=1}^{N} a_j a_m a_p a_q \right. \\ &\quad \left. \times \exp\{\mathrm{i}\mathbf{q}[\mathbf{x}_j(0) - \mathbf{x}_m(0) + \mathbf{x}_p(\tau) + \mathbf{x}_q(\tau)]\}\right\rangle \\ &= N\langle |a|^4\rangle + N(N-1)\langle |a|^2\rangle^2 \\ &\quad \times \{1 + |\langle \exp[\mathrm{i}\mathbf{q}\Delta\mathbf{x}(\tau)]\rangle|^2\} \\ &= N\langle |a|^4\rangle + N(N-1)\langle |a|^2\rangle^2 \\ &\quad \times \{1 + \exp(-2q^2 D\tau)\} . \end{aligned} \tag{51}$$

For a large number of particles in the measurement volume N, (51) simplifies to the Siegert relation [46]

$$g_2(\tau) = G_2(\tau)/\langle n\rangle^2 = 1 + |g_1(\tau)|^2 . \tag{52}$$

This relation generally holds for Gaussian amplitude statistics. The small g will be used for normalized correlations throughout this paper.

For identical, independent particles, (52) predicts a singly exponential decay also for the intensity correlation,

$$g_2(\tau) = 1 + \exp(-2q^2 D\tau) . \tag{53}$$

Compared to the amplitude correlation, (53) shows an additional background and a decay that is faster by a factor of 2.

Real experiments with finite coherence at the detector produce lower contrast in the signal and lead to a reduced second-order correlation

$$g_2(\tau) = 1 + \beta \exp(-2q^2 D\tau) . \tag{54}$$

Even though the intercept β could – in principle – be computed from the optical setup, it is commonly determined from the actually measured correlogram.

The usual evaluation procedure of correlation data involves normalization by the mean count rate or a

very large lag time value of the correlogram ("far point"), subtraction of the background, and a linear regression to the logarithm of $g_2(\tau)-1$. The slope of the fitted line yields the time constant and hence D, its intercept with $\tau=0$ is β.

c) Polydispersity. Of course, quasi-elastic light scattering is not restricted to monodisperse, noninteracting particles. Many real suspensions show polydispersity, i.e. a spread in particle size, and at high concentrations, interactions will always influence the Brownian motion. Both effects lead to a spread in the time constant in (49), which may be modelled by a continuous distribution or by a sum over discrete values.

This distribution of time constants is related to $g_1(\tau)$ by a Laplace transform. $g_2(\tau)$ contains additional cross terms and is hence less suitable for direct polydispersity analysis. The common first step of such an analysis is thus inversion of the Siegert relation (52) to obtain

$$|g_1(\tau)| = [g_2(\tau)-1]^{1/2}. \tag{55}$$

Unfortunately, the Laplace inversion of finite accuracy data constitutes an ill-posed problem [4]. High-frequency components in the distribution of time constants tend to be averaged out by integration over the very smooth Laplace kernel and are easily buried in experimental noise. Hence, they cannot be reconstructed upon inversion. McWhirter and Pike [47] clearly explained this behavior in terms of an eigenfunction analysis of the Laplace transform.

In practice, bimodal size distributions cannot be clearly resolved, if the two peaks are separated by less than a factor of about 2. Still, mean diffusion constants may be determined with about 1% accuracies, even for rather wide particle size distributions [46].

A large number of procedures have been used to invert correlation data. They range from a simple cumulant fit to main frame programs like CONTIN. A recent review was given by Stock and Ray [46]. More details may be found in the papers by Ostrowsky and Sornette, Bertero and Pike, Ford and Chu, Danovich and Serdyuk, as well as Provencher in [4]. Yet the search for reliable procedures still continues and seems to be revived by linear optimization schemes now [48].

A common feature of many inversion schemes is a logarithmic spacing of the time constants in calculated distributions, i.e. grid points are chosen as a geometric series. Eigenfunction theory [47, 4] justifies this choice and even suggests a geometric pattern for the spacing of lag times in the correlation function. Such a channel spacing would optimize the resolution over large lag time ranges with a limited number of channels – and hence limited cost – of the correlator.

First attempts to approximate a geometric lag time spacing by the introduction of suitably spaced delay channels, however, unfortunately sacrificed the noise performance of the instrument [49]. Splitting conventional correlators into up to 4 separate units with different sample times provided a costly but very limited approximation of the ideal geometric spacing.

d) New Structurator/Correlator. A novel correlator architecture was required to provide an increasing width of the sampling time intervals proportional to the geometrically increasing lag time over a large range of times. Only such an increase in sampling interval width would keep the signal-to-noise ratio of a geometrically sampled correlogram at the same level as it would be for a correlogram with constant lag time increment and a very large number of channels [49].

The major benefits of a geometric channel spacing – lower cost of the instrument and less computer time used for inversion procedures – all result from the reduction in the number of channels required to span a certain lag time range. These benefits would be most noticable for a very large range of simultaneous lag times, say a spread like 1:10000 or more.

Based upon fast input data buffering, a new 4 by 4 bit fully parallel pipelined channel design, and a separate 16 bit processor to compute very large lag time channels, I developed an architecture for my digital structurator/correlator [28, 43, 44], which achieves multiple tau operation with up to 23 groups of 8 linearly spaced channels each. The sample time is doubled between adjacent groups, yielding a pseudo geometric structure over a range of more than seven decades of simultaneous lag times, e.g. between 1 μs and several 10 s.

Such an enormous lag time spacing greatly eases the measurement of very wide distributions of time constants, as they are observed in strongly interacting samples [64]. Figure 11 presents as an example the

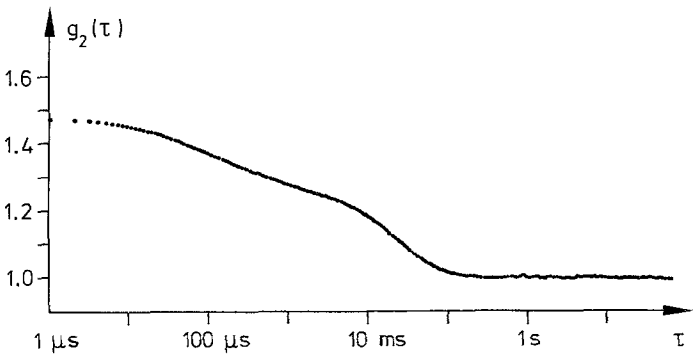

Fig. 11. Photon correlation function measured by homodyne scattering under 20° from strongly interacting latex spheres, covering more than seven decades of lag times in a single run

multiple tau correlogram of a sample, where 50 nm latex particles in deionized water show strong and long-range electrostatic repulsion. The time constants extend over much more than three decades.

Besides offering such an enormous range of simultaneous lag times, the structurator/correlator is the first available instrument able to compute digital structure functions with the same high speed (sample times down to 20 ns, count rates up to 100 MHz) as correlograms. The possibilities offered by the use of photon structure functions instead of correlations – particularly on highly polydisperse systems – are still largely uninvestigated today.

Theoretically expected [26] are improvements, if fast components are to be measured in the presence of slower ones at sufficiently high count rates. Such components, which correspond to small length scale refractive index structures, are typically weak, due to the strong particle size dependence of scattering amplitudes in the Rayleigh regime. These components are often difficult to determine by photon correlation functions.

e) Reference-Beam Measurements. Because of their uncritical setup, single-beam homodyne optics dominate Brownian motion studies. The same measurements may, however, be done with one of the reference beam setups as described in Sect. 1.2, as well.

Advantages in the signal-to-noise ratio and the possibility to reach smaller scattering angles make reference beam or heterodyne techniques preferable, if very large diffusion constants are to be determined. This is the case for studies of thermal diffusion in pure liquids [33] or diffusion of concentration fluctuations in liquid mixtures.

Improvements due to heterodyning should also exist for polydispersity problems, because reference beam techniques yield as an essential contribution to the correlogram the product of reference intensity and the first order or amplitude correlation of the scattered light. Thus there is no need to reduce a second-order correlation to a first-order correlation, a procedure which significantly reduces the signal-to-noise ratio of homodyne measurements at large lag times.

Disadvantages of heterodyne techniques are their high sensitivity to mechanical vibration or convective flows in the sample, as well as particularly stringent requirements for laser stability and absence of afterpulsing in the photo detector. The last problem may be circumvented by cross correlation, at the price of a reduced signal-to-noise ratio [33].

3.2. Velocimetry

a) Laser Doppler Techniques. While the sensitivity of heterodyne experiments to collective particle motion was just a nuisance in diffusion studies, it is the desired effect for the measurement of flow velocities. In the transition regime between both applications we find mobility studies, e.g. on biological systems.

The principle of laser Doppler velocimetry (LDV) was already explained in Sect. 1.2, when we discussed dual beam setups. Velocity information is obtained from the size of the Doppler shift of laser light scattered by small particles (0.5 μm... 5 μm, typically), which move with the flow under study.

Many LDV experiments use symmetric real fringe setups with large aperture incoherent detection, in order to produce strong Doppler signals that are suitable for analog real time processing by counter or tracker systems [11, 50].

More demanding applications, however, like long-range and backscattering setups, or measurements that need extreme accuracy [51], often require the high sensitivity and the statistically correct averaging offered by photon correlation processing.

The typical LDV measurement volume in the crossing region of two laser beams consists of a fringe pattern with Gaussian envelope (Fig. 6). A flow velocity v perpendicular to the fringes produces a normalized and baseline corrected correlogram like

$$g_2(\tau)=\exp(-v^2\tau^2/2R^2)\,[1+\beta\cos(qv\tau)]\,, \tag{56}$$

where R denotes the radius of the measurement volume, q the scattering vector length or 2π/fringe separation, and β is the fringe visibility.

Velocity fluctuations, e.g. due to turbulence, are measurable, if their relative magnitude exceeds the ratio of fringe separation to the diameter of the measurement volume, i.e. for turbulence levels above the inverse number of fringes. With typical systems using some 10... 100 fringes, resolutions between 1% and 10% may be obtained. The correlogram may be computed as a velocity average of (56),

$$g_2(\tau)=\int_0^\infty p(v)\exp(-v^2\tau^2/2R^2)\,[1+\beta\cos(qv\tau)]\,dv\,. \tag{57}$$

Again, an inversion problem must be solved to recover $p(v)$, the velocity distribution. For the simplest case of many fringes, the exponential factor in (57) may be neglected and a straightforward Fourier transformation yields $p(v)$. More sophisticated inversion schemes combine Fourier transforms with corrections for the neglected exponential. Maximum resolution may be obtained by eigenfunction expansions. The papers by Abbiss, Brown, and Inman and Bradbury in [4] contain reviews of the various inversion schemes.

Inversion of photon correlation data is greatly simplified, if the character of $p(v)$ is known a priori as a model distribution, where just a few parameters must be fitted. Gaussian distributions, if necessary modified

by a Gram Charlier series, were used to model turbulence [52] with good success but occasional convergence problems.

Easier than for turbulence, correct models may be formulated for simple periodic flows. For a sinusoidal flow, (57) yields a series of Bessel functions. Using this series up to second-order provided an excellent fit to correlograms measured in a singly periodic Taylor-Couette flow, i.e. the flow between an inner rotating and an outer fixed cylinder. Figure 12 shows an example.

b) Laser Transit Velocimetry. For low turbulence levels, a second laser technique has been established besides LDV. The dual focus or laser transit velocimeter (LTV) uses two narrowly focused parallel laser beams, in order to determine flow velocities from the measurement of the time delay between the crossing times of a single particle, that transverses both beams.

Again, photon correlation is the most suitable technique for long range measurements with low scattered light intensities. A single detector and autocorrelation or a separate detector for each beam and cross correlation may be used. In both cases, the velocity is determined as the ratio of the beam separation and the lag time corresponding to the correlation maximum.

As compared to LDV, LTV allows measurements closer to reflecting and scattering walls, where many technically important flow phenomena are located. More information about laser transit velocimetry may be found in the paper by Brown in [4].

c) Time-Resolved Velocimetry. Analog processors for laser velocimetry signals typically provide real time, instantaneous velocity information (although with a limited accuracy, usually in the 1% region). Photon correlation processing, however, owes its advantages, like the ability to recover a weak signal buried in noise or the statistically correct averaging even at high turbulence levels, to long-time averaging. Hence velocity information from photon correlation systems is typically precise, but time averaged. Even if high signal-to-noise levels allow for short data collection times, there remains the time consuming problem of recovering velocity information from measured correlograms.

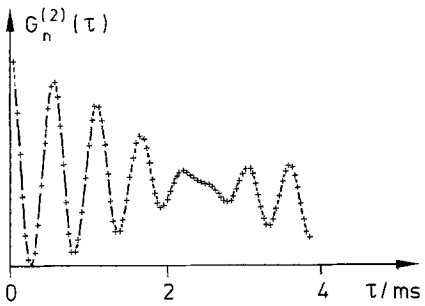

Fig. 12. Photon correlation function measured by the real fringe technique on a rotating Taylor-Couette flow in a region of singly periodic instability (crosses) and model fit (continuous line)

The high cost of a real-time photon correlation velocimeter, e.g. a fast correlator plus a parallel FFT processor for inversion, has restricted the use of such systems to laboratory tests. The inability of simple photon correlation setups to provide real time flow data probably explains, why photon correlation found much less acceptance for velocimetry than for particle sizing applications.

4. Recurrence Rate Correlation

Information about the temporal character of flows, which is so difficult to obtain by photon correlation, may however be determined quite elegantly by a different correlation technique. This technique, now known as rate correlation, allows immediate measurements of temporal velocity correlation functions.

4.1. Single-Beam Rate Correlation

Rate correlation was invented by Erdmann and Gellert [9, 10], who used a simple single beam geometry, as described in Sect. 1.1, with incoherent detection. Of course, such a system is "blind" to Doppler shifts, but it is well suited to count particle transits by comparing the scattered light intensity against a fixed threshold.

Let us consider these particle transit events as our discrete counting signal $n(t)$. Their average rate is proportional to the particle density, the cross section of the observed measurement volume, and the flow velocity $v(t)$. For constant particle concentration we obtain

$$\langle n(t)|v(t)\rangle = Cv(t) \tag{58}$$

with constant C – just our linearity condition (12). If we limit our attention to lag times larger than the longest particle transit time through the measurement volume and assume noninteracting particles, we obtain statistically independent counts $n(t)$ and $n(t+\tau)$ for given velocities – the second one of our two fundamental conditions. Hence we may apply our theory of correlations of a doubly stochastic process and arrive at

$$\langle n(t)n(t+\tau)\rangle = C^2\langle v(t)v(t+\tau)\rangle, \tag{59}$$

proportionality between rate correlation and velocity correlation.

The constant C depends on particle concentration, laser power, detector sensitivity, and the set threshold.

In practice, it must be determined experimentally, if absolute velocity units are required. For many experiments, however, normalized correlation information suffices, and C need not be determined.

The existence of a "forbidden region" at small lag times is typical for rate correlation techniques. It limits temporal resolution just like the finite size of the measurement volume limits spatial resolution. For single-beam rate correlation, the "forbidden region" equal to a particle's transit time shows a strong similarity to the dead-time problem in photon correlation.

Practical advantages of single-beam rate correlation as compared to other optical velocimetry schemes are the extremely simple setup, the use of efficient incoherent detection, and the small bandwidth required for signal processing. These advantages become important for longe-range measurements at large velocities.

Disadvantages are the critical dependence on uniform seeding, the difficult determination of the constant C in (59), and the unusual radial velocity component measured by single-beam rate correlation.

4.2. Cross Beam Rate Correlation

In order to obtain correlations of single Cartesian velocity components, I combined the idea of rate correlation with the conventional symmetric real fringe optics of laser Doppler velocimetry. Incoherent detection and forward scattering produce a strong analog signal. High-pass filtering removes the low-frequency pedestal due to the mean intensity profile in the measurement volume. There remains a pure ac signal of – possibly overlapping – Doppler bursts. The zero crossings of these bursts are the counted events, our rate signal.

a) Low Seeding. At low particle concentrations, we neglect burst overlap, i.e. we ignore situations with more than one particle inside the measurement volume at any one time. Hence the burst arrival rate equals that of single-beam rate correlation, with the exception of a differently shaped measurement volume.

The additional presence of fringes in the measurement volume serves to code the velocity direction. Particles moving in a fringe plane do not produce any zero crossings in the high-pass filtered Doppler signal. Only a velocity component v perpendicular to the fringes contributes to the zero crossing rate. The rate of such crossing events inside a burst equals $2v/s$, if s denotes the fringe separation.

As a result, we obtain a crossing rate proportional to v and hence a rate correlation function

$$\langle n(t)n(t+\tau)\rangle = C^2\langle v(t)v(t+\tau)\rangle \tag{60}$$

for lag times τ outside of the "forbidden region" below the longest particle transit time through the measurement volume. Differentiation between forward and backward flows is, just like in conventional LDV, possible by frequency shifting [12–14]. At the same time, frequency shifting may ease the correct setting of the high pass cutoff frequency. The size of the "forbidden region" is not affected by frequency shifting.

While cross beam rate correlation does measure a more useful Cartesian velocity component, the other disadvantages of single-beam rate correlation, in particular the dependence on uniform seeding, are not overcome at low seed particle concentrations. Complexity of the optical system and processing bandwidth requirements are much higher for the cross beam technique.

b) High Seeding. In the opposite limit of high seeding concentration, we may assume many particles inside the measurement volume all the time. With incoherent detection, we obtain Gaussian intensity statistics. The theory of Gaussian random processes [53] relates the rate of zero crossings to the curvature of the temporal correlation of the high pass filtered Doppler signal,

$$\langle I(t)I(t+\tau)\rangle = \exp(-v^2\tau^2/2R^2)\cos(qv\tau), \tag{61}$$

at lag time zero by

$$\langle n(t)|v(t)\rangle/t_s = 2[(v/s)^2 + (v/2\pi R)^2]^{1/2}. \tag{62}$$

t_s is again used to denote the length of a sampling interval. With typical beam radius values R more than a decade above the fringe separation s, the last term in (62) may be safely neglected. Hence we obtain a zero crossing rate close to twice the Doppler frequency and a rate correlation

$$\langle n(t)n(t+\tau)\rangle = (2t_s/s)^2\langle v(t)v(t+\tau)\rangle. \tag{63}$$

At high seeding, the constant C in (60) approaches a limit, that is given by the scattering geometry alone. The dependence on nonuniform seeding vanishes, we overcome the second disadvantage of single-beam rate correlation.

Particularly with frequency shifting or at small turbulence levels, measured rate signals at high seeding show small fluctuations about their mean only. For such signals, structure functions yield faster and more accurate results than correlations [14, 24]. Furthermore, structure functions may be computed by a simpler algorithm than correlograms, if multi-bit data are processed [19]. Hence, we now prefer the measurement of rate structure functions instead of correlograms, if the flow permits high seeding levels.

If correlators are used to process weakly fluctuating signals, their performance may be greatly improved by a subtracting preprocessor, which reduces each $n(t)$

by a fixed value prior to correlation processing to increase the relative variance [14, 55, 56].

The sensitivity of cross beam rate correlation at moderate seed levels like one particle per measurement volume may be reduced by passing the Doppler signal through an LDV tracker prior to thresholding [13, 56]. The tracker holds the Doppler frequency during short drop outs, but it may cause problems with fast velocity changes. Rate correlograms may become distorted at small lag times, a tracker tends to extend the "forbidden region".

The Taylor-Couette flow again supplies a measurement example. In this case, the cross beam rate correlogram obtained with a tracker clearly shows the presence of two oscillation modes in the flow with some broadening of the fast component (Fig. 13).

Particularly for the investigation of very complex temporal flow patterns in Taylor-Couette flow, I developed a special structure function processor with up to 8000 channels, 8 bit input data format, and real-time operation at sample times below 1 ms as a single board unit to be plugged into a commercial micro computer.

4.3. Noise Considerations

The arrival of seed particles in a measurement volume follows – just like photon counting statistics – essentially a Poisson process. Hence, our noise considerations, although initially formulated for photon correlation only, may be applied to rate correlation as well. The correspondence is obvious for single-beam rate correlation. It may be extended to cross beam correlation, if we treat whole bursts (instead of single threshold crossings) as Poisson events.

Sources of noise are counting noise – due to random particle arrival – and signal noise – due to fluctuations of the measured velocity component. Their relative importance is governed by the number of seed particles arriving within one "coherence time" of the flow velocity, i.e. within the turbulent integral time scale. If this number is of order unity or below, counting noise dominates. In this limit, the seeding level directly determines the measurement accuracy. In the opposite limit of large particle arrival rates, signal noise dominates and not much is to be gained by further increases of the seeding concentration.

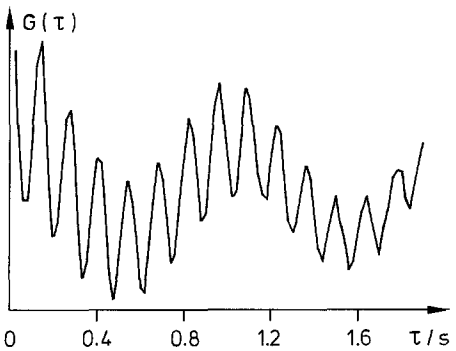

Fig. 13. Rate correlation function measured by a real fringe setup with PLL tracker, showing doubly periodic instability of Taylor-Couette flow

The crossover concentration between both regimes depends on the turbulence level. This behavior is quite analogous to the noise performance of reference beam experiments in photon correlation. Both cases may be modelled by Gaussian statistics of the underlying process. While counting noise is essentially determined by the mean value of the underlying process, signal noise is – by definition – equal to its variance. For a Poisson counting process, we obtain a crossover concentration proportional to the inverse relative variance of the signal, i.e. the square of the inverse turbulence level.

If experimentally feasible, the seeding level should be chosen above this crossover, in order to ensure maximum accuracy of the measured rate correlogram. If the seed level is so high as to keep the average number of particles in the measurement volume above one, we also have the benefit of knowing the constant of proportionality in (60), independent of the absolute value of the seed particle concentration. While in this limit the noise analogy to photon correlation breaks down due to severe burst overlap, this typically happens well above the cross-over concentration for a well designed experiment, where the noise level has already become independent of the seeding concentration.

Depending on the dominating type of noise, we should decide, whether to use structure function or correlation processing. Below the crossover concentration, with dominating counting noise, correlograms provide better signal-to-noise ratios. Above this limit, where signal fluctuations prevail, we are typically better off with structure functions.

Noise considerations as well as the desire for easy absolute calibration of measured rate correlograms lead to high seed levels as optimum condition for cross beam rate correlation. In this regime, no other technique – like post processing of real-time LDV data – can provide more accurate velocity correlation information than rate correlation, simply because there is no way to avoid the very signal fluctuations which are to be determined by the measurement. With its two advantages of full real-time performance and absence of bias problems [63], rate correlation (or the calculation of rate structure functions) constitutes an ideal measuring technique for the study of temporal fluctuations in flows, which tolerate high seeding.

5. Phase Structure Function

So far, our attention has been restricted to the measurement of optical amplitudes and intensities obtained in dynamic light scattering experiments. These signals carry velocity information encoded as Doppler-frequency shifts. Completely new signal processing techniques may, however, be based upon direct measurements of optical phase signals. This section will describe such a technique, which is able to resolve very small collective particle motions otherwise obscured by diffusion broadening.

5.1. Single Particle Phase Statistics

For a single scattering particle, phase changes ϕ are directly related to the particle displacement x. We may rewrite (2) as

$$u_D = |u_D| \exp(i\phi) = a \exp(i\mathbf{q} \cdot \mathbf{x}) \tag{64}$$

or

$$\phi = \mathbf{q} \cdot \mathbf{x}. \tag{65}$$

Hence, measurements of the phase statistics immediately yield particle displacement statistics. For the case of Brownian motion, we obtain a mean square change or phase structure function

$$D_\phi(\tau) = \langle \Delta\phi^2 \rangle = q^2 \langle \Delta x^2 \rangle = 2q^2 D\tau. \tag{66}$$

As already discussed in Sect. 2.2, the correlation function of such a nonstationary phase signal is not well defined. We are forced to use structure functions (or other moments of phase differences) in this application.

For constant particle motion with velocity v, we obtain a quadratic rise of the phase structure function,

$$D_\phi(\tau) = q^2 v^2 \tau^2. \tag{67}$$

Periodic particle motion with

$$x(t) = x_0 + \Delta x \sin(\Omega t) \tag{68}$$

leads to a periodic phase structure function,

$$D_\phi(\tau) = q^2 \Delta x^2 [1 - \cos(\Omega\tau)]. \tag{69}$$

In the simultaneous presence of more than one of the types of particle motion discussed above, the corresponding phase structure functions add up. This fact makes the measurement of phase structure functions a suitable technique for the simultaneous determination of diffusional and very small collective particle motion.

Such measurements are severely limited with "classical" laser Doppler techniques, because – in the case of photon-correlation processing – the measured correlogram falls off like a negative exponential due to diffusion. Hence, collective particle motion components cannot be detected if they are too weak to produce a significant fraction of at least one full Doppler cycle within the diffusional decay time. For periodic particle motion, intensity processing techniques typically do not succeed, if the peak-to-peak displacement falls below one fringe separation.

In contrast, phase structure functions allow the simultaneous determination of diffusion and collective motion over large ranges of their relative magnitudes, because both types of motion lead to additive contributions in the phase structure function which coexist (and do not vanish) even for lag times much larger than the decay time in the corresponding photon correlogram. Particularly the possibility of resolving much smaller collective particle motions otherwise completely obscured by diffusion indicates the practical importance of the concept of phase structure functions.

5.2. Many-Particle Phase Statistics

Unfortunately, the simple relation between optical phase and particle displacement gets lost, if we consider multi particle scattering. Coherent addition of single particle amplitudes leads to the random walk picture already used in Sect. 1.1b. Destructive interference occasionally causes almost vanishing signal amplitudes. Since the magnitude of complex amplitude changes is essentially independent of the current amplitude value, such a situation produces arbitrarily large phase changes within very short lag times.

For a large number of scattering particles, the absolute amplitude of the signal follows a Rayleigh distribution [32]. Its probability density falls off linearly towards zero for small amplitudes A. With phase changes of order $1/A$, i.e. squared phase changes of order $1/A^2$, integration over small amplitudes results in a logarithmic divergence – the phase structure function is not well defined!

However, weighting of phase changes by the instantaneous absolute amplitude leads to a well behaved stochastic process,

$$Q(\tau) = \int_0^\tau A(t) d\phi(t) = \int_0^\tau A(t) \dot{\phi}(t) dt, \tag{70}$$

the tangential change of the complex signal

$$A(t) \exp[i\phi(t)] = \sum_{j=1}^{N} a_j \exp[i\varphi_j(t)], \tag{71}$$

where a_j and $\varphi_j(t)$ denote amplitude and phase of the single particle contributions and N is the number of particles in the measurement volume. Temporal changes of the a_j are again neglected as slow compared to the $\varphi_j(t)$ [57].

In the presence of diffusive and collective particle motion, phases may be split into a pure diffusion term

(index D) and a pure collective term (index C). The collective term is the same for all particles and we obtain

$$\varphi_j(t)=\varphi_j^D(t)+\varphi^C(t), \tag{72}$$

$$\phi(t)=\phi^D(t)+\varphi^C(t). \tag{73}$$

In the random walk picture, diffusion leads to a "boiling" of the single particle contributions, while collective motion results in a simple rotation of the whole random walk graph about the origin of the complex plane. It should be noted that only diffusion causes changes in the absolute amplitude $A(t)$. Hence, we may treat the pure diffusion problem,

$$A(t)\exp[\mathrm{i}\phi^D(t)]=\sum_{j=1}^{N} a_j\exp[\mathrm{i}\varphi_j^D(t)], \tag{74}$$

separately first.

a) Pure Diffusion. Taking the temporal derivative of (74) and multiplying with $\exp(-\mathrm{i}\phi^D)$, we obtain

$$\dot{A}(t)+\mathrm{i}A(t)\dot{\phi}^D(t)=\sum_{j=1}^{N}\mathrm{i}a_j\dot{\varphi}_j^D(t)\exp[\mathrm{i}\varphi_j^D(t)-\mathrm{i}\phi^D(t)] \tag{75}$$

with the imaginary part

$$A(t)\dot{\phi}^D(t)=\sum_{j=1}^{N} a_j\dot{\varphi}_j^D(t)\cos[\mathrm{i}\varphi_j^D(t)-\mathrm{i}\phi^D(t)]. \tag{76}$$

For Brownian motion of noninteracting particles, the $\dot{\varphi}_j^D(t)$ are random varibles, which are independent of each other and of all the instantaneous phases and amplitudes. On time scales which are – as in this application – several orders of magnitude larger than hydrodynamic relaxations, particle velocities and hence our $\dot{\varphi}_j^D(t)$ are delta correlated with

$$\langle\dot{\varphi}_j^D(t)\dot{\varphi}_j^D(t+\tau)\rangle=2q^2D\delta(\tau). \tag{77}$$

From (76) and (77) we obtain the diffusion term of the amplitude weighted-phase structure function (AWPS),

$$\begin{aligned}
D_{Q^D}(\tau)&=\langle\Delta Q^D(\tau)^2\rangle\\
&=\left\langle\int_0^\tau\int_0^\tau A(t)\dot{\phi}^D(t)A(t')\dot{\phi}^D(t')dt\,dt'\right\rangle\\
&=\sum_{j=1}^{N}\sum_{m=1}^{N}\int_0^\tau\int_0^\tau\langle a_ja_m\rangle\\
&\quad\times\langle\cos[\varphi_j^D(t)-\phi^D(t)]\cos[\varphi_m^D(t')-\phi^D(t')]\rangle\\
&\quad\times\langle\dot{\varphi}_j^D(t)\dot{\varphi}_m^D(t')\rangle dt\,dt'\\
&=N\int_0^\tau\langle a^2\rangle\langle\cos^2[\varphi_j^D(t)-\phi^D(t)]\rangle 2q^2D\,dt\\
&=\langle A^2\rangle q^2D\tau.
\end{aligned} \tag{78}$$

In the last line of (78) we used the identities

$$\langle A^2\rangle=N\langle a^2\rangle \tag{79}$$

and

$$\langle\cos^2[\varphi_j^D-\phi^D]\rangle=1/2. \tag{80}$$

Equation (80) holds for large N only, where the two phases considered show a vanishing dependence.

The diffusion term of the AWPS agrees with that of the phase structure function of a single particle (66) except for the additional factor $\langle A^2\rangle$. This factor is determined by a monitor channel during the measurement of the AWPS, and may then be divided out for proper normalization.

b) Collective Motion. The calculation of the collective motion term in AWPS is slightly more complicated and we will state the starting equation and some important results only. Since the amplitude $A(t)$ does not depend on collective motion, we obtain two separate averages,

$$\begin{aligned}
D_{Q^C}(\tau)&=\langle\Delta Q^C\langle\tau\rangle^2\rangle\\
&=\int_0^\tau\int_0^\tau\langle A(t)A(t')\rangle\langle\dot{\varphi}^C(t)\dot{\varphi}^C(t')\rangle dt\,dt'\\
&=\int_{-\tau}^{\tau}\langle A(t)A(t+\tau')\rangle\langle\dot{\varphi}^C(t)\dot{\varphi}^C(t+\tau')\rangle|\tau'|d\tau'.
\end{aligned} \tag{81}$$

The correlation of the absolute amplitude may be computed as [21]

$$\begin{aligned}
\langle A(t)A(t+\tau)\rangle&=(\pi/4)\langle A^2\rangle[1-\varrho(\tau)^2]\\
&\quad\times F[3/2,3/2;1,\varrho(\tau)^2],
\end{aligned} \tag{82}$$

where

$$\varrho(\tau)=\exp(-q^2D\tau). \tag{83}$$

F denotes a hypergeometric series [58]. While (82) seems complicated, it just describes a smooth decay of the absolute amplitude correlation from an initial value $\langle A^2\rangle$ to its large lag time limit

$$\langle A\rangle^2=\langle\pi/4\rangle\langle A^2\rangle. \tag{84}$$

Equation (82) is time dependent through $\varrho(\tau)$ only. Hence this decay occurs for lag times of the order $1/q^2D$. If we consider much larger lag times, we may use the approximation

$$\langle A(t)A(t+\tau)\rangle\approx\langle A\rangle^2, \tag{85}$$

which simplifies the solution of (81) to

$$D_{Q^C}(\tau)=(\pi/4)\langle A^2\rangle D_{\varphi^C}(\tau). \tag{86}$$

For the periodic motion of (68), this relation reads

$$D_{Q^C}(\tau)=(\pi/4)\langle A^2\rangle q^2\Delta x^2[1-\cos(\Omega\tau)]. \tag{87}$$

Again, the AWPS essentially agrees with the single-particle phase structure function.

5.3. *Experimental Techniques*

Although our theory was stated in terms of complex amplitudes for ease of understanding, reference beam setups for the direct measurement of such amplitudes are useful at very large particle concentrations only. For moderate concentrations (typically up to some 1000 per measurement volume), symmetric real fringe systems with incoherent detection yield better signal-to-noise ratios as already discussed in Sect. 1.2.

Due to the analogy between the high-pass filtered Doppler signal of real-fringe systems and one component of the complex amplitude obtained by coherent scattering from a single laser beam, all calculations of the preceding sections remain applicable.

In a first AWPS system, we used Bragg cell frequency shifting and time measurements of zero crossings of the high-pass filtered Doppler signal for phase detection. 16 bits of phase with 8 bits [21, 23, 57] or 12 bits [22, 23] in 2π yielded phase information with a resolution of about 0.01 rad. Box-car integration of the absolute value of the amplitude of the filtered Doppler signal over a full period and 8 bit analog-to-digital conversion supplied the required instantaneous amplitude information. A microprocessor or a mini computer calculated phase differences, amplitude weighting and the final structure function. Assember programs were used to achieve real time operation for sample times down to 1 ms. 64 simultaneous lag time channels were typically determined [21].

A second AWPS system now uses another scheme of direct detection of amplitude weighted phase differences, which is illustrated in Fig. 14. Each zero crossing of the filtered Doppler signal starts a timer that first triggers a peak measurement after a quarter period of the shift frequency. This peak measurement serves to determine the instantaneous amplitude. After a full period of the shift frequency, the filtered Doppler signal is sampled again. For a phase difference of zero, this sample would coincide with the next zero crossing. For phase differences small compared to 1 rad, we obtain an almost linear dependence of phase change and sampled signal. The factor of proportionality is nothing but the absolute amplitude. Hence, our second sample is the desired amplitude weighted phase change.

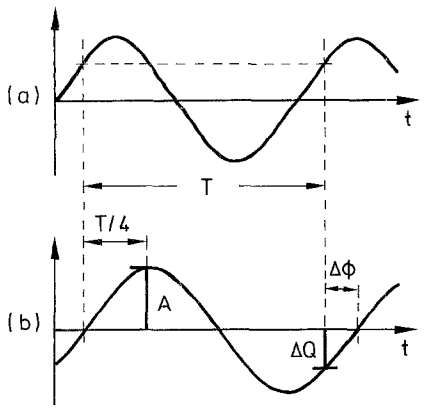

Fig. 14. Direct sampling scheme for amplitude (A) and amplitude weighted phase change (ΔQ) based upon signal samples taken at times equal to a quarter and a full period (T) of the frequency shift signal (a) past a zero crossing of the filtered Doppler signal (b)

The measurement of both samples with the same 10 bit analog-to-digital converter reduces systematic normalization errors of the structure function, which is again computed on a micro or mini computer in real time [57].

There are two major experimental difficulties. Firstly, the sensitivity of up to 1/1000th of a fringe results in extreme requirements of mechanical stability and vibration isolation. Furthermore, all beams have to be shielded against thermal air turbulence.

Secondly, the frequency shift between the two laser beams must be of exceptional quality. For dual Bragg cell shifting, particular problems arise if there is any cross talk between the two drivers. Although contained in the otherwise low-frequency pedestal, this cross talk component falls at the center of the desired signal bandwidth and may thus not be removed by filtering. Its relative magnitude becomes amplified by the ratio of pedestal to Doppler signal, i.e. essentially by the square root of the number of scattering particles in the measurement volume. Thus amplification by a factor as large as 100 may occur, rising sub-1% driver cross talk to intolerable magnitude. Being a fixed component, cross talk tends to reduce the measured phase changes and to decrease the values obtained for diffusion constants and velocities.

Our setups use a specially designed Bragg cell drive unit, where the shift frequency is directly input from an external generator. While simplifying the phase detection, this approach requires very careful calibration to achieve the desired low cross talk levels. Other driver schemes and alternative means of frequency shifting are still under investigation in our laboratory.

5.4. *Histogram Measurements*

Even more information than from the AWPS may be obtained from simultaneous measurements of histograms of $\Delta Q(\tau)$ at various lag times. The AWPS as well as higher moments of amplitude weighted phase differences are easily computed from such a set of histograms.

Furthermore, contributions due to a constant velocity motion like drift or convection, may be completely eliminated by resorting to central moments. This scheme reduces the sensitivity of measurements to such disturbancies.

Our present experiment allows the real time measurement of 64 histograms with 256 bins each and a bin capacity of 32 bits. Data are sampled every 1 ms, the lag time increment may be any integer multiple of this time. A 65th channel is used to obtain absolute amplitude histograms. These serve for normalization and – by comparison with the theoretical Rayleigh distribution – as a measure of signal quality and dust problem monitor.

The measurement of higher-order moments is useful, if the particles do not show identical collective motion, but rather a distribution of motion amplitudes. If diffusion is not too strong, moments of such distributions may be calculated from higher order moments of amplitude-weighted phase changes.

Finally we plan the measurement of histograms of ΔQ multiplied by the sign of the (externally stimulated) collective motion. This scheme again reduces the influence of drifts and convection, at least for a symmetric stimulated motion. In addition, motion amplitudes may be measured by first-order moments for improved accuracy.

5.5. *Applications in Electrophoresis*

My development of AWPS techniques was motivated by the desire to improve the sensitivity of electrophoretic light scattering experiments, i.e. the measurement of particle motion in an electric field. Although such measurements are widely performed with conventional LDV techniques [60, 61], diffusion broadening severely restricts their use with samples of small mobility and samples which do not tolerate large field strengths, e.g. due to Joule heating.

While it is generally realized that periodic fields reduce problems like electrolysis, field frequencies have to be kept very small (typically below 1 Hz), to avoid a loss in spectral resolution [62]. Essentially, conventional LDV techniques require a particle motion exceeding the fringe separation.

First AWPS measurements, on the other hand, yielded reasonable mobility data for particle oscillation by as little as 10 nm peak-to-peak. This was less than 1/100th of the fringe separation and about 1/30th of the particle diameter. Hence, macro emulsion droplets with a zeta potential of 40 mV could be measured with an effective field strength as low as 0.6 V/cm and a field frequency as high as 50 Hz [21].

Further increases in sensitivity may be obtained by a reduction of the field frequency and the transition to histogram measurements.

6. Conclusions

New signal processing techniques significantly increase the use of dynamic light scattering experiments for the study of small particle motion. This holds for well established techniques like photon correlation, which may be used to investigate extremely polydisperse samples with multiple tau processing, as well as for novel processing schemes like rate correlation or AWPS measurements, which access additional motion parameters – like velocity correlations – or provide large sensitivity enhancements – like in the case of electrophoretic mobilities.

All of the mentioned techniques are based upon the temporal analysis of stochastic measured data by correlation or structure functions. Their principle of operation and their noise performance can be derived from a general discussion of doubly stochastic processes and particular statistical models like the Poisson and the Gamma process.

First successes of the new signal processing techniques are accurate diffusion measurements of strongly interacting samples in several laboratories [64], which use the high resolution and the large range of lag times provided by my structurator/correlator design, numerous rate correlation measurements, which helped to clarify complex transitions of Taylor-Couette flow from the laminar region into turbulent chaos [15, 16], and the use of phase structure functions for pharmaceutical investigations of electrophoretic mobilities [65].

Acknowledgements. For continuing support and discussion of my work I have to thank Prof. E. O. Schulz-DuBois and all my collaborators at Kiel, particularly Dr. J. Merz, Dr. M. Drewel, S. Faber, C. Harbers, S. Schröder, B. Stampa und J. Ahrens. The final development of my structurator/correlator was the result of an extremely fruitful cooperation with Ing. W. H. Peters of ALV, Langen.

Thanks for stimulating discussions also go to Prof. E. R. Pike, Prof. E. Jakeman, Prof. Simonsohn, Dr. G. Parry, Dr. G. Pfister, Dr. P. Hille, Dr. T. Mullin, and Dr. Y. Georgalis as well as to all other collegues, who took an interest in my work at Malvern or at Kiel. Financial support of the 'Deutsche Forschungsgemeinschaft' is gratefully acknowledged.

References

1. H.Z. Cummins, E.R. Pike (eds.): *Photon Correlation and Light Beating Spectroscopy* (Plenum, New York 1974)
2. B.J. Berne, R. Pecora: *Dynamic Light Scattering* (Wiley, New York 1976)
3. H.Z. Cummins, E.R. Pike (eds.): *Photon Correlation Spectroscopy and Velocimetry* (Plenum, New York 1977)
4. E.O. Schulz-DuBois (ed.): *Photon Correlation Techniques in Fluid Mechanics*, Springer Ser. Opt. Sci. **38** (Springer, Berlin, Heidelberg 1983)
5. R. Hanbury-Brown, R.Q. Twiss: Nature **177**, 27 (1956)
6. R. Foord, E. Jakeman, R. Jones, C.J. Oliver, E.R. Pike: IEE Conf. Proc. **14** (1969)
7. R. Foord, E. Jakeman, C.J. Oliver, E.R. Pike, R.J. Blagrove, E. Wood, A.R. Peacocke: Nature **227**, 242 (1970)

8. K. Schätzel: Appl. Phys. B **41** (1986)
9. J.C. Erdmann, R.P. Gellert: J. Opt. Soc. Am. **68**, 787 (1978)
10. J.C. Erdmann, R.P. Gellert: Physica Scripta **19**, 396 (1979)
11. R. Vehrenkamp, K. Schätzel, G. Pfister, B.S. Pfister, E.O. Schulz-DuBois: Physica Scripta **19**, 379 (1979)
12. R. Vehrenkamp, K. Schätzel, G. Pfister, E.O. Schulz-DuBois: J. Phys. E **12**, 119 (1979)
13. K. Schätzel: Optica Acta **27**, 45 (1980)
14. K. Schätzel: In [Ref. 4, p. 226]
15. T. Mullin, T. Brooke Benjamin, K. Schätzel, E.R. Pike: Phys. Lett. **83A**, 333 (1981)
16. G. Pfister, U. Gerdts, A. Lorenzen, K. Schätzel: In [Ref. 4, 256]
17. K. Schätzel: Opt. Lett. **5**, 389 (1980)
18. K. Schätzel, G. Parry: Optica Acta **29**, 1441 (1982)
19. K. Schätzel: Fluktuationen der optischen Weglänge in turbulenten Phasenobjekten, Dissertation, Univ. Kiel (1982)
20. K. Schätzel: J. Opt. Soc. Am. **73**, 269 (1983)
21. K. Schätzel, J. Merz: J. Chem. Phys. **81**, 2482 (1984)
22. K. Schätzel, M. Drewel, J. Merz, S. Schröder: Inst. Phys. Conf. Ser. **77**, 185 (1985)
23. J. Merz: Messungen von Diffusionskonstanten und elektrophoretischen Beweglichkeiten in hochdispersiven Systemen mit Hilfe der Amplitudengewichteten Phasenstrukturfunktion, Dissertation, Univ. Kiel (1985)
24. E.O. Schulz-DuBois, I. Rehberg: Appl. Phys. **24**, 323 (1981)
25. C.J. Oliver, E.R. Pike: Optica Acta **29**, 1345 (1982)
26. K. Schätzel: Optica Acta **30**, 155 (1983)
27. K. Schätzel: 2nd Intl. Conf. on Trends in Quantum Electronics, Bucharest (1985)
28. K. Schätzel: Inst. Phys. Conf. Ser. **77**, 175 (1985)
29. W. Feller: *An Introduction to Probability Theory and its Applications*, 2nd ed. (Wiley, New York 1971) Vol. 2
30. C. Keveloh, W. Staude: Appl. Opt. **22**, 333 (1982)
31. C. Keveloh, W. Rümelin, W. Staude: Inst. Phys. Conf. Ser. **77**, 171 (1985)
32. B. Saleh: *Photoelectron Statistics*, Springer Ser. Opt. Sci. **6** (Springer, Berlin, Heidelberg 1978)
33. G. Hiller, G. Simonsohn: In [Ref. 4, 377]
34. E.O. Schulz-DuBois, H. Koppe, R. Brummer: Appl. Phys. **21**, 369 (1980)
35. M. Drewel: Zur inkohärenten Streuung von Laserlicht an Teilchenzahlfluktuationen, Diplomarbeit, Univ. Kiel (1982)
36. E. Jakeman, E.R. Pike, S. Swain: J. Phys. A **3**, 255 (1970)
37. E. Jakeman, E.R. Pike, S. Swain: J. Phys. A **4**, 517 (1971)
38. C.J. Oliver: J. Phys. A **12**, 591 (1979)
39. I. DeLotto, P.F. Manfredi, P. Principe: Energia Nucl. **11**, 557 (1964)
40. E. Jakeman, C.J. Oliver, E.R. Pike: J. Phys. A **4**, 827 (1971)
41. S.K. Srinivasan, M. Singh: Phys. Lett. **8**, 409 (1981)
42. K. Schätzel: Festschrift zum 60. Geburtstag von E. O. Schulz-DuBois, ed. G. Pfister, Kiel (1986)
43. ALV-3000 User's Manual, ALV Laser GmbH, Langen, FRG (1985)
44. K. Schätzel: Conf. on Quasi Elastic Light Scattering Spectra, Worcester, Mass. (1986)
45. H.Z. Cummins, H.L. Swinney: *Progr. Opt.* **8** (North-Holland, Amsterdam 1970)
46. A.J.F. Siegert: MIT Rad. Lab. Report No. 465 (1943)
47. J.G. McWhirter, E.R. Pike: J. Phys. A **11**, 1729 (1978)
48. K. Zimmermann, M. Delaye: Conf. Physical Optics of Dynamic Phenomena und Processes in Macromolecular Systems, Prague (1984) p. 54
49. E.O. Schulz-DuBois: Photon Correlation, lecture at Viana do Castelo, Portugal (1984)
50. B.S. Fedders, A. Köneke: J. Phys. E **12**, 765 (1979)
51. R. Vehrenkamp: Nach dem Photonen-Korrelations-Verfahren durchgeführte Laser-Doppler-Messungen zur Wirbelentstehung in gekrümmten Kanälen, Dissertation, Univ. Kiel (1981)
52. A.D. Birch, D.R. Brown, J.R. Thomas: J. Phys. D **8**, 438 (1875)
53. S.O. Rice: Selected Papers on Noise and Stochastic Processes, ed. by N. Wax (Dover, New York 1954)
54. K. Schätzel: Ratenkorrelation – Ein neues Messverfahren zur zeitlichen Analyse stationärer Strömungen, Diplomarbeit, Univ. Kiel (1979)
55. K. Schätzel: Appl. Phys. **22**, 251 (1980)
56. K. Schätzel, E.O. Schulz-DuBois, R. Vehrenkamp: Optics and Laser Technology, 91 (April 1981)
57. M. Drewel: Intensitäts- und Phasenfluktuationsspektroskopie von Laserstreulicht aus Interferenzstreifensystemen in Suspensionen, Dissertation, Univ. Kiel (1985)
58. I.S. Gradshteyn, I.M. Ryzhik: *Table of Integrals, Series, and Products* (Academic, New York 1980) p. 1039
59. Constructed by P. Hille, Kiel (1983)
60. A.J. Bennet, E.E. Uzgiris: Phys. Rev. A **8**, 2662 (1973)
61. B.H. Ware, W.H. Flygare: Chem. Phys. Lett. **12**, 81 (1971)
62. R.S. Stock, W.H. Ray, J. Polymer Sc.: Polymer Phys. Ed. **23**, 1393 (1985)
63. D.K. McLaughlin, W.G. Tiederman: Phys. Fluids **16**, 2082 (1973)
64. M. Wenzel, W. Burchard, K. Schätzel: Polymer **27**, 195 (1986)
65. B.W. Müller, J. Merz, R.H. Müller: Colloid and Polymer Sci. **263**, 342 (1985)
66. N. Wiener: Acta Math. **55**, 117 (1930)
67. A. Einstein: Ann. Phys. **17**, 549 (1905)